[1]H. S. W. Massey and A. H. A. Moussa, Proc. Phys. Soc. (London) 72, 38 (1958).
[2]K. Smith, W. F. Miller, and A. J. P. Mumford, Phys. Rev. 76, 559 (1960).
[3]P. G. Burke and H. M. Schey, Phys. Rev. 126, 147 (1962).
[4]W. J. Cody, J. Lawson, H. S. W. Massey, and K. Smith, Proc. Roy. Soc. (London) 278A, 479 (1964).
[5]L. Spruch and L. Rosenberg, Phys. Rev. 117, 143 (1960).
[6]D. C. S. Allison, H. A. J. McIntyre, and B. L. Moiseiewitsch, Proc. Phys. Soc. (London) 78, 1169 (1961).
[7]C. Schwartz, Phys. Rev. 124, 1468 (1961).
[8]H. S. W. Massey and C. B. O. Mohr, Proc. Phys. Soc. (London) 67A, 695 (1954).
[9]M. F. Fels and M. H. Mittleman, Phys. Rev. 163, 129 (1967).
[10]B. H. Bransden and Z. Jundi, Proc. Phys. Soc. (London) 92, 880 (1967).
[11]J. F. Dirks and Y. Hahn, Phys. Rev. A 3, 310 (1971).
[12]G. Doolen, G. McCartor, F. A. McDonald, and J. Nuttall, Phys. Rev. A 4, 108 (1971).
[13]G. J. Seiler, R. S. Oberoi, and J. Callaway, Phys. Rev. A 3, 2006 (1971).
[14]M. Rotenberg and J. Stein, Phys. Rev. 182, 1 (1969).
[15]A different set of transformed tail functions was proposed by J. C. Y. Chen and M. H. Mittleman [Ann. Phys. (N. Y.) 37, 269 (1966)] and used in Ref. 9.
[16]R. K. Nesbet, Phys. Rev. 179, 60 (1969).
[17]C. Schwartz, Ann. Phys. (N. Y.) 16, 36 (1961).
[18]A. K. Bhatia, A. Temkin, R. J. Drachman, and E. Eiserike, Phys. Rev. A 3, 1328 (1971).
[19]S. K. Houston and R. J. Drachman, Phys . Rev. A 3, 1335 (1971).

PHYSICAL REVIEW A VOLUME 6, NUMBER 6 DECEMBER 1972

Electron-Impact Excitation and Ionization of Atomic Oxygen*

P. A. Kazaks, P. S. Ganas,† and A. E. S. Green
University of Florida, Gainesville, Florida 32601

(Received 29 June 1972)

We utilize the analytic atomic independent-particle model (IPM) of Green, Sellin, and Zachor to calculate generalized oscillator strengths (GOS) and total cross sections for excitation and ionization of atomic oxygen. First we average over the experimental energy levels within a multiplet to arrive at single-particle levels. Then we adjust the two parameters of the IPM potential so that it accurately characterizes the ground state and 15 lowest excited states. Using the wave functions so obtained, and assuming the Born approximation and the *LS*-coupling scheme, we calculate absolute GOS and cross sections for excitation to these levels, and for ionization with incident energies up to 1000 eV and secondary electron energy up to 200 eV. We obtain an analytic representation of the excitation GOS as a function of the momentum transfer. We also obtain an analytic representation of the energy differential cross section for ionization as a function of the energies of the incident and secondary electrons. Comparison is made with available experimental data and other calculations.

I. INTRODUCTION

Because of the importance of atomic oxygen in the upper atmosphere (it is the predominant species above 150 km), it is essential for an understanding of aeronomical phenomena to have a reliable characterization of its properties. Of particular interest to the understanding of auroral, dayglow, and ionospheric phenomena are electron-impact cross sections. Unfortunately, because of difficulties in working with atomic oxygen, there is little experimental information available on important cross sections.

From a theoretical point of view, atomic oxygen plus the electron constitutes a nine-electron system. Techniques for treating such systems rigorously have not yet been reduced to practice. For this reason, the present theoretical calculation exploits a realistic independent-particle-model (IPM) description for arriving at approximate electron-impact cross sections in the Born–Bethe approximation.

In comparison to Hartree–Fock–Slater calculations and to experiment, a simple two-parameter IPM potential has been found to provide a good representation of atoms[1] and electron-atom interactions.[2–5] We apply the IPM to the excitation and ionization of oxygen.

II. EXPERIMENTAL LEVELS AND IPM POTENTIAL

The ground state of oxygen has the configuration

$$1s^2 2s^2 2p^4 (^3P_2) . \qquad (1)$$

From the tables of Moore,[6] it can be seen that of the 44 excited states below the ionization limit which are listed, 40 of them are in the configuration

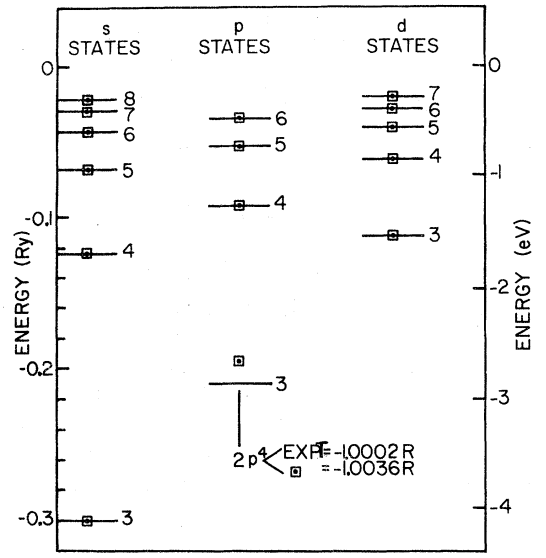

FIG. 1. Excited-state energies of oxygen. The lines denote average of experimental levels. The symbol ⊡ denotes theoretical IPM energy levels based upon parameters $d = 0.8164$ and $H = 2.224$.

$$1s^2 2s^2 2p^3(^4S_{3/2})nl \ . \tag{2}$$

In other words, the active electron is coupled to a ^4S core. We will only consider such states, where the core is in a ^4S state. A given configuration gives rise to a triplet and quintet state very close to each other. Since the ground state is a triplet, we can only reach with direct interaction excited states that are triplets. We will only consider the 15 lowest excited states since the five highest ones are very close to each other just below the ionization limit. These 15 states have configurations $2p^3(^4S)\,3s$-$8s$, $2p^3(^4S)3p$-$6p$, and $2p^3(^4S)\,3d$-$7d$.

Since the IPM cannot distinguish between different states lying within a given multiplet, we replace each multiplet by an average value, as discussed in Sec. II of Ref. 3. The averages so obtained serve as the experimental single-particle levels. The parameters d and H for the IPM potential[3] were determined by searching on the 15 experimental energies and the ground-state ionization energy. In Fig. 1 we present the experimental levels and the calculated levels corresponding to $d = 0.8164$ and $H = 2.224$. We see that the experimental levels are fitted quite well by our model. It might be added that the quintet states would fall on top of the triplet states to within plotting accuracy in Fig. 1, except for the $3p$ state. In Table I, we present the quantum defects for oxygen based on the averages of the experimental levels. The quantum defect δ_l is defined by

$$E_{nl} = -(n - \delta_l)^{-2} \text{ (in Ry)}, \tag{3}$$

where E_{nl} is the single-particle energy.

III. FORMULAS FOR EXCITATION GENERALIZED OSCILLATOR STRENGTHS

Following the formulation and notation of Ganas and Green,[3] we consider the transition of an atom from its ground state to an excited state with momentum transfer K. We define $x = K^2 a_0^2$, where a_0 is the Bohr radius and $x_t = W/R$, where W is the energy loss and R is the Rydberg energy. We shall also make considerable use of the reduced or scaled quantity

$$\xi = x/x_t = (K^2/W)\, a_0^2 R \ . \tag{4}$$

We suppose that the atom is initially in a state specified by the quantum numbers L_i, S_i, J_i, M_i. After the active electron has been promoted from a $n_0 l_0$ orbital to a nl orbital, the atom is in a final state specified by the quantum numbers L_f, S_f, J_f, M_f. We note that the possible values of L_f are determined by the coupling $\vec{L}_f = \vec{L}_c + \vec{l}$, where L_c designates the core. The possible values of J_f are determined by the coupling $\vec{J}_f = \vec{L}_f + \vec{S}_f$. We consider only transitions with $S_f = S_i$.

Using the Born approximation and the Russell–Saunders LS-coupling scheme,[7] it can be shown that (see Appendix A) the generalized oscillator strength (GOS) is given by

$$f(x) = \sum_L C_L (2l_0 + 1)(2l + 1)(2L + 1) \begin{pmatrix} l_0 & l & L \\ 0 & 0 & 0 \end{pmatrix}^2 S_L^{\,2} \ , \tag{5}$$

where

$$S_L = \xi^{-1/2} \int_0^\infty R_{n_0 l_0}(r)\, j_L(Kr)\, R_{nl}(r)\, r^2\, dr \tag{6}$$

and

$$C_L = N C_{FP}^2 \,(2L_i + 1)(2L_f + 1)(2J_f + 1) \times \begin{Bmatrix} L_f & L & L_i \\ l_0 & L_c & l \end{Bmatrix}^2 \begin{Bmatrix} J_i & L & J_f \\ L_f & S_i & L_i \end{Bmatrix}^2 . \tag{7}$$

The array in the large parentheses in Eq. (5) is a $3j$ symbol, while the arrays in curly brackets in Eq. (7) are $6j$ symbols.[8] The functions $R_{n_0 l_0}(r)$ and $R_{nl}(r)$ are the bound-state radial wave functions for the single-particle excitations, and $j_L(Kr)$ is a spherical Bessel function. The quantity N in Eq. (7) is the total number of electrons in the active subshell, and the quantity C_{FP} is the "coefficient of fractional parentage."[9] The summation index

TABLE I. Quantum defects for oxygen.

	s	p	d
δ_l	1.174	0.797	0.020

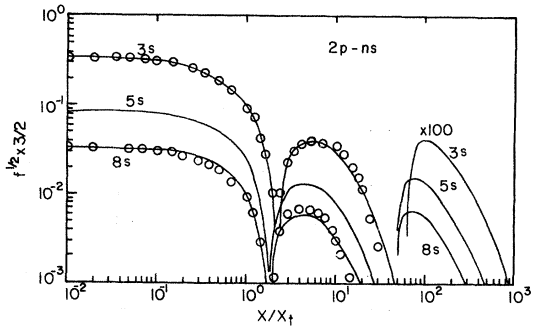

FIG. 2. Curves indicating oscillator amplitude $\sqrt{f}$ vs reduced square of momentum transfer $\xi = x/x_t$, for $2p \rightarrow ns$ transitions in oxygen. The circles represent an analytic fit using Eq. (13).

L in Eq. (5) is required to satisfy the following three conditions:

$$|J_i - J_f| \leq L \leq J_i + J_f \,, \tag{8}$$

$$|l_0 - l| \leq L \leq l_0 + l \,, \tag{9}$$

$$l_0 + l + L \text{ is even.} \tag{10}$$

It is interesting to note that Eq. (5) is very similar to Eq. (18) of Ref. 3. The main difference is the fact that the coefficient C_L was treated as an adjustable parameter in Ref. 3, while in the present work it is given by an explicit formula, Eq. (7), based on LS coupling.

Equations (5)–(7) are general formulas within the framework of the Born approximation and the LS-coupling scheme. If we consider excitations from the $2p$ subshell in oxygen, we have, for a ^4S core,

$$C_{FP} = [p^4(^3P)|p^3(^4S)] = -1/\sqrt{3} \,. \tag{11}$$

In addition, $NC_{FP}^2 = \frac{4}{3}$, $l_0 = 1$, $L_c = 0$, $L_i = 1$, $S_i = 1$, $J_i = 2$, $L_f = l$. Substituting these values into Eqs. (5) and (7) and summing over J_f, we obtain

$$f(x) = \tfrac{4}{3}(2l+1)\sum_L (2L+1)\begin{pmatrix} 1 & l & L \\ 0 & 0 & 0 \end{pmatrix}^2 S_L{}^2 \,. \tag{12}$$

Equation (12) is an expression for the GOS (summed over J_f) for excitations from the $2p$ subshell in oxygen, assuming a ^4S core.

IV. RESULTS FOR EXCITATION

We have calculated the GOS from Eq. (12) for the allowed transitions $2p \rightarrow 3s$-$8s$ and $2p \rightarrow 3d$-$7d$, and the forbidden transitions $2p \rightarrow 3p$-$6p$, for the range $0.01 \leq \xi \leq 900$. Some representative curves are shown in Figs. 2–4. The curves have a nodal structure similar to that obtained in calculations with the rare gases.[3,10] The excitation GOS calculated by McGuire[11] using approximate Hartree–Fock–Slater wave functions is close to our results.

To expedite use in applications, we have parametrized all our GOS results with simple analytic forms. For transitions to s and d states, the following analytic expression gives good fits to the GOS:

$$\phi(\xi) \equiv (f(\xi))^{1/2} = \phi_0 (e^{-\alpha\xi} + \beta\xi e^{-\gamma\xi}) \,. \tag{13}$$

For transitions to p states we use

$$\phi(\xi) \equiv (f(\xi))^{1/2} = \phi_0 \{\xi/[(1+\alpha\xi)(1+\beta\xi+\gamma\xi^2)]\}^{1/2} \,. \tag{14}$$

We have not attempted to fit the GOS over the whole range of ξ; values of ξ beyond which the GOS has fallen to at least 10^{-4} of its largest value were not considered. In considering transitions to s and d states, we did not vary the parameter ϕ_0; rather, ϕ_0 was determined by extrapolating to $\xi = 0$, and was then left fixed. We identify ϕ_0^2 as the optical oscillator strength. The parameter ϕ_0 was allowed to vary in the case of transitions to p states. Thus, we obtain three-parameter fits to the GOS for transitions to s and d states and four-parameter fits for transitions to p states. The best fits are indicated by small circles in

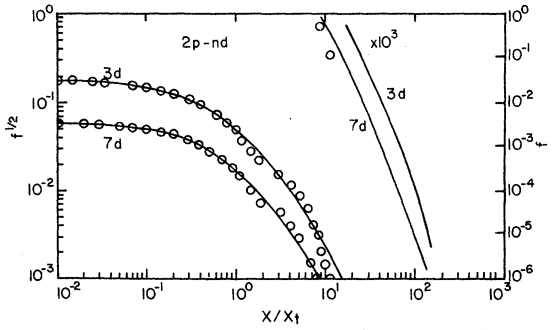

FIG. 3. Curves for $2p \rightarrow nd$ transitions in oxygen. (See caption to Fig. 2.)

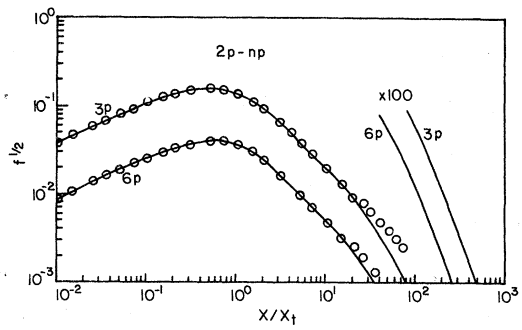

FIG. 4. Curves for $2p \rightarrow np$ transitions in oxygen. The analytic fits are based on Eq. (14).

TABLE II. Parameters for analytic amplitudes, Eqs. (13) and (14).

$2p$ to	ϕ_0	α	β	γ	$100\chi^2$
$3s$	0.2363	1.129	−0.056	0.182	1.0
$4s$	0.0945	0.989	−0.122	0.250	1.4
$5s$	0.0559	0.940	−0.150	0.271	1.3
$6s$	0.0384	0.920	−0.164	0.281	1.1
$7s$	0.0285	0.905	−0.174	0.288	1.0
$8s$	0.0223	0.893	−0.183	0.294	0.9
$3d$	0.1768	1.648	0.124	0.507	1.1
$4d$	0.1270	1.598	0.124	0.505	0.9
$5d$	0.0937	1.552	0.115	0.486	0.8
$6d$	0.0723	1.538	0.113	0.483	0.7
$7d$	0.0577	1.530	0.114	0.485	0.6
$3p$	0.3845	4.51	−0.507	0.891	1.2
$4p$	0.1938	4.17	−0.733	0.943	1.2
$5p$	0.1241	3.89	−0.758	0.958	0.9
$6p$	0.0885	3.69	−0.753	0.967	0.7

Figs. 2–4. In Table II we list the values of the parameters obtained in fitting all the GOS. Also given are $100\chi^2$ obtained when the weight $1/\phi$ is used for each point. Using Table II and Eqs. (13) and (14), we can accurately generate GOS for the range of ξ in which the GOS is significant.

The practical aspects of our study of GOS arise from its usefulness in providing cross sections. The cross sections and the GOS are related by standard formulas.[3,12] The parametric forms (13) and (14) lead to a total cross section in closed form. In Fig. 5 we present some representative cross sections. The experimental data on excitation cross sections for atomic oxygen are rather sparse. We have found only one measurement of an excitation cross section for atomic oxygen in the literature.[13] This experiment on the excitation of the $3s(^3S)$ resonance state is carried out up to 150-eV incident electron energy. An extremely sharp peak near 20 eV is observed and is attributed to cascade processes. The values of the $2p$-$3s$ cross section given in Fig. 5 in the range 50–150 eV are all about one-half of the experimental result. This difference may be due to the contribution of a variety of cascade processes to the experimental result.

We have examined the rule for optical oscillator strengths in Rydberg series,

TABLE III. Values of parameters δ and ϕ^* in Eq. (15) for the three transition series in oxygen.

Transitions	δ	ϕ^*
$2p \rightarrow ns$	1.74	0.33
$2p \rightarrow nd$	−0.66	1.25
$2p \rightarrow np$	1.22	0.91

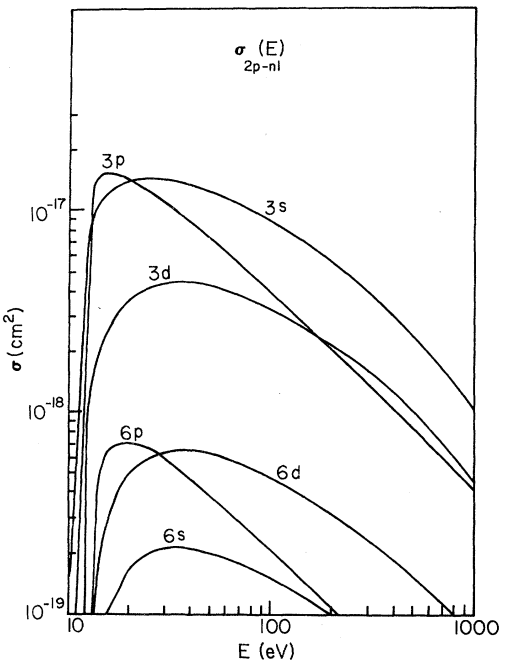

FIG. 5. Representative excitation cross sections for oxygen. The curves are based upon our analytic representation of the Born GOS.

$$\phi_0 = \phi^*/(n-\delta)^{3/2}, \tag{15}$$

which has been suggested in previous studies.[3,12,14] We find that Eq. (15) gives a good fit to the values of ϕ_0 given in Table II. The best values of ϕ^* and δ are given in Table III.

Finally, we discuss the optical oscillator strength which, of course, is the GOS in the limit of zero momentum transfer. In Table IV we present our calculated values based on our IPM wave functions. Also included for comparison in Table IV are the results of Kelly[15] using Hartree–Fock–Slater wave functions, and McGuire[11] using approximations to Hartree–Fock–Slater wave functions. Our results

TABLE IV. Optical oscillator strengths for transitions in oxygen.

$2p$ to	This work	Kelly (Ref. 15)	McGuire (Ref. 11)
$3s$	0.056	0.059	0.106
$4s$	0.008	0.008	0.019
$5s$	0.003	0.002	0.007
$6s$	0.0015	0.0008	•••
$7s$	0.0008	0.0004	•••
$8s$	0.0005	0.0002	•••
$3d$	0.0313	0.027	0.044
$4d$	0.0161	0.019	0.022
$5d$	0.0088	0.013	•••
$6d$	0.0052	0.0079	•••
$7d$	0.0033	0.0051	•••

TABLE V. Experimental oscillator strengths for the $2p$-$3s$ resonance transition in oxygen.

Reference	Oscillator strength
16	0.033
17	0.033
18	0.023
19	0.18
20	0.044
21	0.035
22	0.050
23	0.046
This work	0.056

generally lie close to Kelly's. The differences between the results of the various calculations may reflect the sensitivity of optical oscillator results to fine details of the radial wave functions. There appears to be an abundance of experimental data on the $3s(^3S)$ resonance state. In Table V we give a list of experimental determinations of the $2p$-$3s$ oscillator strength. It is clear from Table V that the experimental values vary appreciably. Our calculated value is centrally located with respect to these determinations.

V. FORMULAS FOR IONIZATION GOS

In considering collisions in which the incident electron ionizes the target atom, we use the same prescription to describe this process as in the case of discrete excitations. Specifically, we assume that the incident electron interacts with the atom according to the Born approximation. One $2p$ electron is ejected into the continuum. The final-state wave function of the ejected electron is now a continuum wave function in our analytical potential. As such, it has an infinite number of orbital angular momentum components rather than one specific one as in the case of discrete excitations. Herein lies one major difference and complication of the ionization problem. Another difference from the discrete case is that the ejected electron can have a continuum of energies rather than one specific one. After integrating over the angles of the ejected electron, we arrive at a differential cross section which is now a double differential cross section. It is differential in the final angles of the incident electron and in the energy loss, i.e., $d^2\sigma/d\Omega\, dW$. We note that $W = T + I$, where T is the energy of the ejected electron and I is the binding energy of the ground state.

We consider an ionization process in which an electron in the $n_0 l_0$ subshell is ejected into the continuum with a momentum $\vec{k}'$. Let the initial and final momenta of the projectile electron be $\vec{k}_0$ and $\vec{k}$, respectively, and let $\vec{K} = \vec{k}_0 - \vec{k}$ be the momentum transfer. We suppose that the target atom is initially in a state specified by the quantum numbers L_0, S_0, J_0, M_0. After ionization, the residual atom, or "core," is in a state specified by the quantum numbers L_c, S_c, J_c, M_c. By using the Born approximation and the Russell–Saunders LS-coupling scheme,[7] it can be shown that (see Appendix B) in atomic units

$$\frac{d^2\sigma}{d\Omega\, dW} = \frac{4}{K^4}\,\frac{k}{k_0}\,\frac{1}{\pi k'}\,NC_{\mathrm{FP}}^2\,(2S_0+1)\,(2L_0+1)(2J_c+1)$$

$$\times\sum_j (2j+1)\begin{Bmatrix} S_0 & L_0 & J_0 \\ S_c & L_c & J_c \\ \frac{1}{2} & l_0 & j \end{Bmatrix}^2 \sum_{l'} (2l'+1)\sum_l (2l+1)\begin{pmatrix} l' & l & l_0 \\ 0 & 0 & 0 \end{pmatrix}^2 |g^l_{l'l_0}|^2 , \quad (16)$$

where

$$g^l_{l'l_0} = \int_0^\infty R_{l'}(k'r)\, j_l(Kr)\, R_{n_0 l_0}(r)\, r^2\, dr . \quad (17)$$

In Eq. (17), $R_{l'}(k'r)$ is the radial component of the l'th partial wave of the continuum wave function, and is obtained by solving the radial Schrödinger equation with the same analytic IPM potential as the initial state. In Eq. (16), the array in the large parentheses is a $3j$ symbol, while the array in the large curly brackets is a $9j$ symbol.[8] In Eqs. (16) and (17), the quantities N, C_{FP} and the functions $j_l(Kr)$, $R_{n_0 l_0}(r)$ have the same interpretations as in Sec. III. In Eq. (16), j takes the values $l_0 + \frac{1}{2}$ and $l_0 - \frac{1}{2}$, while l' runs from 0 to ∞ and l runs from $|l' - l_0|$ to $l' + l_0$.

The continuum GOS is defined by

$$\frac{d^2\sigma}{d\Omega\, dW} = 4\,\frac{k}{k_0}\,\frac{1}{K^2}\,(df/dW)/W . \quad (18)$$

From Eqs. (16) and (18) we obtain for the continuum GOS

$$\frac{df}{dW} = \frac{BW}{\pi k' K^2}\sum_{l'} (2l'+1) \times\sum_l (2l+1)\begin{pmatrix} l' & l & l_0 \\ 0 & 0 & 0 \end{pmatrix}^2 |g^l_{l'l_0}|^2 , \quad (19)$$

where the coefficient B is given by the expression

$$B = N C_{\mathrm{FP}}^2 (2S_0+1)(2L_0+1)(2J_c+1) \times \sum_j (2j+1) \begin{Bmatrix} S_0 & L_0 & J_0 \\ S_c & L_c & J_c \\ \frac{1}{2} & l_0 & j \end{Bmatrix}^2 . \quad (20)$$

Equation (19) is a general formula for the continuum GOS within the framework of the Born approximation and the LS-coupling scheme. It is similar in form to Eq. (5) for the excitation GOS; the major difference lies in the sum over the orbital angular momenta of the ejected electron.

In discussing the excitation of atomic oxygen, we assumed that the core remains in a ^4S state. However, in the ionization process for oxygen, we will take into account all the possible core states: $^4S_{3/2}$, $^2P_{1/2}$, $^2P_{3/2}$, $^2D_{3/2}$, and $^2D_{5/2}$. The relative contributions to the GOS and total ionization cross section from these cores are determined by the coefficient B in Eq. (19). The values of B are listed in Table VI. If we take Eq. (20) and perform a sum over J_c by using the orthogonality property of $9j$ symbols, we arrive at the result

$$\sum_{J_c} B = N C_{\mathrm{FP}}^2 , \quad (21)$$

which is consistent with the results of Table VI. We conclude that the cores ^4S, ^2P ($=^2P_{1/2}+^2P_{3/2}$), and ^2D ($=^2D_{3/2}+^2D_{5/2}$) give contributions to the GOS and total cross section which are, respectively, in the ratio 4:3:5. This ratio is readily obtained from the tables of coefficients of fractional parentage given in Ref. 9. It follows that we need only calculate the contribution from the ^4S core; then we multiply by a factor 3 to obtain the total cross section. As noted in Sec. III, the right-hand side of Eq. (21) is $\frac{4}{3}$ for a ^4S core. Finally, we have an expression for the GOS for ionization from the $2p$ subshell in oxygen, which is analogous to Eq. (12) for the excitation GOS:

$$\frac{df}{dW} = \frac{4}{3}\frac{W}{\pi k'^2 K^2} \sum_{l'} (2l'+1) \times \sum_l (2l+1) \begin{pmatrix} l' & l & l_0 \\ 0 & 0 & 0 \end{pmatrix}^2 |g^l_{l',l_0}|^2 . \quad (22)$$

TABLE VI. Values of B, Eq. (20), for different core states in the ionization of atomic oxygen from the $2p$ subshell.

Core	B
$^4S_{3/2}$	$\frac{4}{3}$
$^2P_{1/2}$	$\frac{1}{6}$
$^2P_{3/2}$	$\frac{5}{6}$
$^2P_{1/2}+^2P_{3/2}$	1
$^2D_{3/2}$	$\frac{1}{6}$
$^2D_{5/2}$	$\frac{3}{2}$
$^2D_{3/2}+^2D_{5/2}$	$\frac{5}{3}$

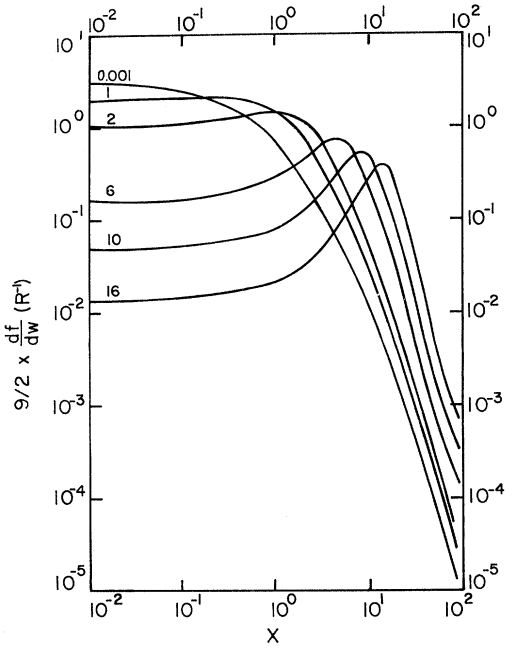

FIG. 6. Ionization GOS for oxygen as a function of x for fixed values of T. The numbers labeling the curves are the values of T in Ry.

VI. RESULTS FOR IONIZATION

Using Eq. (22), and restricting the sum over l' to the first 14 values, we have computed the GOS for values of x in the range $0 < x < 77$ and for values of T in the range $0.001 < T < 16$ Ry. The latter range corresponds to $1 < W < 17$ Ry. In Fig. 6 are shown curves of df/dW for the two extreme values of T and some representative values in between. This figure then represents a series of cuts through the Bethe surface. Similar curves have been obtained in electron-impact ionization studies of the rare gases using the present approach.[5]

The differential ionization cross section $d\sigma/dW$ can be obtained from Eq. (18) by integrating out the angular dependence. If E is the incident electron energy, then

$$S(E, W) \equiv \frac{d\sigma}{dW} = \frac{4\pi}{WE} \int_{x_l}^{x_u} \left(\frac{df}{dW} \Big/ x \right) dx , \quad (23)$$

where

$$x_{u,l} = 2E \left[1 \pm \left(1 - \frac{W}{E} \right)^{1/2} - \frac{W}{2E} \right] . \quad (24)$$

If we take the function $S(E, W)$ and express W in terms of T, we obtain a function of E and T which

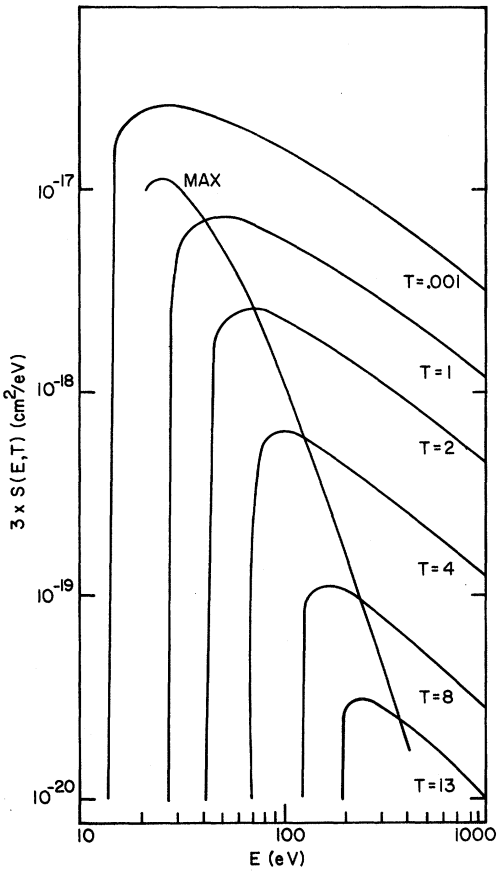

FIG. 7. Secondary-electron distribution for oxygen as a function of incident electron energy for fixed values of secondary-electron energy (T in Ry). The curve labeled MAX represents the function T_{max}, Eq. (25).

we write as $S(E, T)$. This function gives the secondary-electron distribution. We present the computed secondary-electron distributions in Figs. 7 and 8. In Fig. 7, $S(E, T)$ is presented as a function of E for fixed values of T, while in Fig. 8, it is presented as a function of T for fixed values of E. According to our model the secondary electron can have any energy up to $E-I$. However, this is not realistic since the incident electron would have zero energy at this limit. If we make the assumption that the most energetic electron emerging is by definition the primary electron, then the secondary electron has at most the energy

$$T_{max} = \tfrac{1}{2}(E-I) \ . \tag{25}$$

The T_{max} curve is shown in Figs. 7 and 8. The meaningful parts of these figures lie to the right-hand side of the T_{max} curve in Fig. 7 and to the left-hand side in Fig. 8.

The total ionization cross section is obtained using

$$\sigma(E) = \int_I^{(E+I)/2} S(E, W)\, dW \ . \tag{26}$$

To facilitate the numerical integration in Eq. (26), we have parametrized the differential cross section with the analytic form

$$S(E, W) = \frac{\alpha(1 - W/E)\,(1 + \beta E^{1/2}/W)}{E(1 + \gamma W + \delta W^2)} , \tag{27}$$

where α, β, γ, and δ are adjustable parameters. For values of E in the range $55 < E < 1000$ eV and values of W in the range $1 < W < 14$ Ry [subject to $W < \frac{1}{2}(E+I)$], we have obtained 115 points to be fitted with the form (27). The best fits are represented by circles in Fig. 8, and the corresponding parameter values are $\alpha = 0.70$, $\beta = 0.25$, $\gamma = -0.57$, and $\delta = 0.42$ if W, E are expressed in Ry and S is expressed in cm^2/eV. This fit gives $100\chi^2 = 0.8$ when the weight $1/S$ is used for each point.

Finally, the computed total ionization cross sections are shown in Fig. 9. The experimental data are taken from the compilation of Kieffer.[27] The solid line, which represents the results of the present calculations, includes multiplication by a factor 3, representing the contributions from all possible core states as discussed in Sec. V. The over-all agreement between the present results and the experimental data is rather good. Above 100-eV incident electron energy, the present results are centrally located with respect to the two sets of experimental data and are moderately close

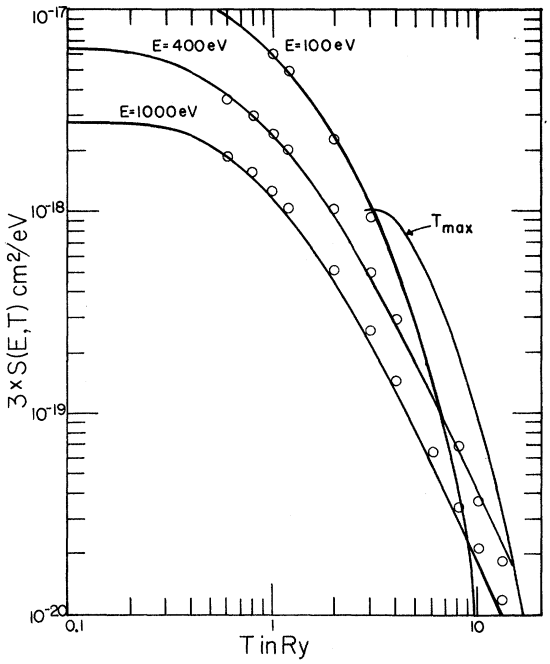

FIG. 8. Secondary-electron distribution for oxygen as a function of secondary-electron energy for fixed values of incident electron energy. The curve labeled T_{max} corresponds to Eq. (25).. The circles represent parametric fits to the distribution curves using Eq. (27).

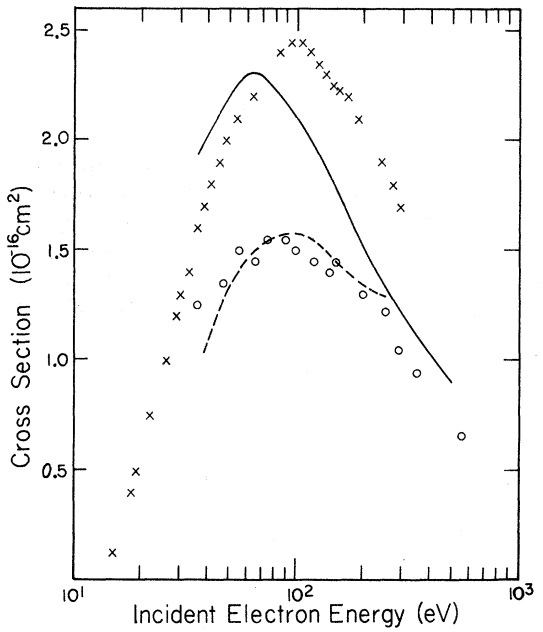

FIG. 9. Total ionization cross sections for oxygen. Experimental data points O and × are from Refs. 24 and 25, respectively. Solid curve represents the results of our IPM calculation, while broken curve represents the theoretical results of Ref. 26.

to the theoretical results of Seaton[26] using Hartree–Fock methods.

In Sec. V we showed that the cores ^4S, ^2P, and ^2D give contributions which are, respectively, in the ratio 4 : 3 : 5. This ratio is confirmed by the high-energy results of Seaton.[26] This ratio is expected to hold only if the ionization process is fast compared to a period necessary for any rearrangement of the electronic structure. This situation occurs only when the outgoing electron is sufficiently energetic.

VII. DISCUSSION

As we indicated in the Introduction, atomic oxygen plays a major role in a number of important atmospheric phenomena which require for their explanation a detailed knowledge of electron-impact cross sections for excitation and ionization. It is still premature to undertake rigorous many-body calculations of such properties which would be valid at all energies. The present approach utilizes a simple analytic independent-particle model which is quite close to the Hartree–Fock–Slater model. Here, however, we can utilize certain aspects of the phenomena in question, in particular the energy levels, to tune up the parameters of the model. In the present instance we have adjusted these parameters to the ground electronic state and 15 excited electronic states of the atom to a high degree of precision. Our calculations lead to reasonable excitation and differential ionization cross sections and total ionization cross sections. On the other hand, experimental data are primarily available for the total ionization cross sections for comparison with the data. Thus the fact that our model gives reasonable results in the Born region in this latter instance lends credence to the excitation and differential ionization cross sections which also are attendant to this model.

In addition to replacing the many-electron system by an independent-particle model, we have pursued our work in the Born approximation. However, if results are needed at low energies (e.g., below 100 eV), rules are available based upon a phenomenological analysis of experimental data[12] for approximately modifying our results. We also have under way a study using the distorted-wave Born approximation to make a more rigorous allowance for the distortion of the incident plane waves in the field of the oxygen atom. The present work serves as a basic starting point for such calculations.

ACKNOWLEDGMENTS

The writers are indebted to Dr. Tatsuro Sawada for his derivations of Eqs. (5) and (16). We also wish to thank R. A. Berg for permission to adapt his ionization code.

APPENDIX A: DERIVATION OF FORMULA FOR EXCITATION GOS

In what follows, the quantum numbers L_i, M_{L_i}, S_i, M_{S_i}, J_i, M_i specify the initial state of the target atom, and L_f, M_{L_f}, S_f, M_{S_f}, J_f, M_f specify the final state. The differential cross section for the scattering of an electron by an atom is

$$\frac{d\sigma}{d\Omega} = \left(\frac{m_e}{2\pi\hbar^2}\right)^2 \frac{k}{k_0} \frac{1}{2J_i+1} \sum_{M_i M_f} |A_{fi}^{M_f M_i}|^2 . \quad \text{(A1)}$$

This is exactly correct if the interaction is spin independent, and we consider only transitions with $S_f = S_i$. In (A1), $\vec{k}_0$ and $\vec{k}$ are, respectively, the initial and final momenta of the projectile electron.

The scattering amplitude is given in the Born approximation by

$$A_{fi}^{M_f M_i} = \left\langle e^{i\vec{k}\cdot\vec{r}} \psi_f(J_f, M_f) \times \left| \sum_{j=1}^{Z} \frac{e^2}{|\vec{r} - \vec{r}_j|} \right| \psi_i(J_i, M_i)\, e^{i\vec{k}_0\cdot\vec{r}} \right\rangle . \quad \text{(A2)}$$

In (A2), ψ_i and ψ_f are the initial- and final-state wave functions, respectively, of the target atom, and Z is the atomic number. According to the well-known expression due to Bethe, (A2) may be

written as

$$A_{fi}^{M_f M_i} = \frac{4\pi e^2}{K^2}\left\langle \psi_f(J_f, M_f)\left|\sum_{j=1}^{Z} e^{i\vec{K}\cdot\vec{r}_j}\right|\psi_i(J_i, M_i)\right\rangle , \quad (A3)$$

where $\vec{K}=\vec{k}_0-\vec{k}$ is the momentum transfer. Using the Rayleigh expansion for $e^{i\vec{K}\cdot\vec{r}}$, (A1) becomes

$$\frac{d\sigma}{d\Omega} = \left(\frac{m_e}{2\pi\hbar^2}\right)^2 \frac{k}{k_0}\,\frac{4\pi}{2J_i+1}\sum_L |g_{J_i J_f L}|^2, \quad (A4)$$

where

$$g_{J_i J_f L} = \frac{4\pi e^2}{K^2}\,\frac{(2J_f+1)^{1/2}}{\langle J_i M L 0 | J_f M\rangle} \times\left\langle \psi_f\left|\sum_p j_L(Kr_p)\, Y_{L0}(\hat{r}_p)\right|\psi_i\right\rangle . \quad (A5)$$

In (A4), L runs from $|J_i - J_f|$ to $J_i + J_f$. In (A5), the quantity $\langle J_i M L 0 | J_f M\rangle$ is a Clebsch–Gordan coefficient. We have chosen $M_i = M_f = M$ and $M_L = 0$. The evaluation of $g_{J_i J_f L}$ depends on the coupling scheme. We consider the Russell–Saunders LS-coupling scheme. The antisymmetric initial state is given by

$$\psi_i = \sum_{M_{S_i} M_{L_i}} \langle S_i M_{S_i} L_i M_{L_i} | J_i M\rangle \sum_{S_1 L_1} C_{\rm FP} \sum_{\substack{M_{S_1} M_{L_1} \\ m_{s_0} m_{l_0}}} \langle S_1 M_{S_1} \tfrac{1}{2} m_{s_0} | S_i M_{S_i}\rangle \times \langle L_1 M_{L_1} l_0 m_{l_0} | L_i M_{L_i}\rangle\, \psi((n_0 l_0)^{N-1} S_1 L_1 M_{S_1} M_{L_1})\, \psi(n_0 l_0 m_{s_0} m_{l_0}), \quad (A6)$$

where $C_{\rm FP}$ is the coefficient of fractional parentage,

$$C_{\rm FP} = [(n_0 l_0)^{N-1}(S_1 L_1)(n_0 l_0) S_i L_i | (n_0 l_0)^N S_i L_i]. \quad (A7)$$

In (A6), $\psi((n_0 l_0)^{N-1} S_1 L_1 M_{S_1} M_{L_1})$ describes the antisymmetric wave function of the core electrons in a $(n_0 l_0)^{N-1}$ configuration with spin and orbital angular momentum S_1 and L_1, respectively. The wave function $\psi(n_0 l_0 m_{s_0} m_{l_0})$ describes the extra core electron which is in a $n_0 l_0$ state and couples to the core to produce the initial state of the atom. The particle in $\psi(n_0 l_0 m_{s_0} m_{l_0})$ can be any one of 1 through N electrons.

For the final state $(n_0 l_0)^{N-1} nl$, the antisymmetrization is done explicitly:

$$\psi_f = \sum_{M_{S_f} M_{L_f}} \langle S_f M_{S_f} L_f M_{L_f} | J_f M\rangle \sum_{\substack{m_s m_l \\ M_{S_c} M_{L_c}}} \langle S_c M_{S_c} \tfrac{1}{2} m_s | S_f M_{S_f}\rangle \langle L_c M_{L_c} l m_l | L_f M_{L_f}\rangle \times N^{-1/2}\left(1 - \sum_{j=2}^{N} P_{1j}\right) \psi((n_0 l_0)^{N-1} S_c L_c, M_{S_c} M_{L_c}; 234\cdots N)\, \psi(nl m_l m_s; 1). \quad (A8)$$

In (A8), P_{1j} is the permutation operator for electrons 1 and j. The wave function $\psi((n_0 l_0)^{N-1} S_c L_c, M_{S_c} M_{L_c}; 234\cdots N)$ describes the core with spin S_c and orbital angular momentum L_c coupled to an electron described by $\psi(nl m_l m_s; 1)$ to produce the final state of the atom.

Since ψ_i and ψ_f as given by (A6) and (A8) are antisymmetric with respect to 1 through N electrons, $\sum_p j_L(Kr_p) Y_{L0}(\hat{r}_p)$ in (A5) can be replaced by $N j_L(Kr_1) Y_{L0}(\hat{r}_1)$. Substituting (A6) and (A8) into (A5), and separating the spatial components of the single-particle wave functions into radial and angular parts, and taking advantage of all orthogonalities, we finally obtain (aside from a phase factor)

$$g_{J_i J_f L} = (4\pi e^2/K^2)(\sqrt{N})\,\delta_{S_i S_f}\, C_{\rm FP}\,[(2l_0+1)(2L+1)/4\pi]^{1/2}\langle l_0 0 L 0 | l 0\rangle\,[(2L_i+1)(2L_f+1)]^{1/2} \times \begin{Bmatrix} L_f & L & L_i \\ l_0 & L_c & l \end{Bmatrix} [(2J_i+1)(2J_f+1)]^{1/2} \begin{Bmatrix} J_i & L & J_f \\ L_f & S_i & L_i \end{Bmatrix} \langle R_{nl}(r)\,|\, j_L(Kr)\,|\, R_{n_0 l_0}(r)\rangle . \quad (A9)$$

In (A9) the arrays in the curly brackets are $6j$ symbols. Equation (5) now follows after inserting (A9) in (A4), and using

$$f(x) = \frac{k_0}{4k}\,\frac{K^4 a_0^2}{\xi}\,\frac{d\sigma}{d\Omega} . \quad (A10)$$

APPENDIX B: DERIVATION OF FORMULA FOR IONIZATION GOS

In this Appendix we give a derivation of Eq. (16) based on the Born approximation and LS coupling. The differential ionization cross section is given

by

$$\frac{d^2\sigma}{dW d\Omega} = \left(\frac{m_e}{2\pi\hbar^2}\right)^2 \frac{k}{k_0} \frac{1}{2J_0+1} \frac{m_e k'}{8\pi^3\hbar^2} \times \sum_{M_0 M_c m_s} \int d\Omega_{\vec{k}'} |\mathfrak{M}|^2 , \quad \text{(B1)}$$

where

$$\mathfrak{M} = \left\langle \mathcal{A}\left[\phi_{\vec{k}'}^{m_s} \Phi_c(L_c S_c J_c M_c)\right] e^{i\vec{k}\cdot\vec{r}} \times \left| \sum_{j=1}^{N} \frac{e^2}{|\vec{r}-\vec{r}_j|} \right| \psi_0(L_0 S_0 J_0 M_0)\, e^{i\vec{k}_0\cdot\vec{r}} \right\rangle . \quad \text{(B2)}$$

Here W is the energy loss, $\vec{k}_0$ is the initial momentum and $\vec{k}$ is the final momentum of the projectile electron, $\Phi_c(L_c S_c J_c M_c)$ is the wave function of the core, $\psi_0(L_0 S_0 J_0 M_0)$ is the wave function of the atom initially, and $\phi_{\vec{k}'}^{m_s}$ is the wave function of the ejected electron in the continuum, which is normalized as in

$$(2\pi)^{-3} \int \phi_{k'}^{*}(\vec{r})\, \phi_{k''}(\vec{r})\, d\vec{r} = \delta(\vec{k}' - \vec{k}'') . \quad \text{(B3)}$$

Corresponding to the experimental situation where the ejected electron is not observed, we integrate over the angles of $\vec{k}'$ in (B1). The average over initial and sum over final spin substates are done in (B1). The symbol $\mathcal{A}$ in (B2) is for antisymmetrization. It is assumed here that Φ_c and ψ_0 are already antisymmetrized. However, the antisymmetrization between the incident and target electrons is not considered. Thus no exchange effects are included.

Using Bethe's formula we find

$$\mathfrak{M} = N(4\pi e^2/K^2)\, I , \quad \text{(B4)}$$

where

$$I = \langle \mathcal{A}\left[\phi_{\vec{k}'}^{m_s} \Phi_c(L_c S_c J_c M_c)\right] | e^{i\vec{K}\cdot\vec{r}_1} | \psi_0(L_0 S_0 J_0 M_0) \rangle . \quad \text{(B5)}$$

We have used the fact that both ψ_0 and $\mathcal{A}[\phi_{\vec{k}'}\, \Phi_c]$ are antisymmetric with respect to N target electrons to replace $\sum_j$ in (B2) by the factor N. Using (B4) in (B1), we find (in atomic units)

$$\frac{d^2\sigma}{dW d\Omega} = \frac{4}{K^4} N^2 \frac{kk'}{k_0} \frac{1}{2J_0+1} \sum_{M_0 M_c m_s} \int d\Omega_{\vec{k}'} \frac{|I|^2}{16\pi^3} . \quad \text{(B6)}$$

The initial-state wave function is the antisymmetrized and angular momentum coupled sum of the one-electron wave function and the core wave function:

$$\psi_0(L_0 S_0 J_0 M_0) = \sum_{M_{S_0} M_{L_0}} \langle S_0 M_{S_0} L_0 M_{L_0} | J_0 M_0 \rangle \sum_{S_c L_c} (C_{\mathrm{FP}})_{S_c L_c}^{S_0 L_0} \times \sum_{M_{S_c} M_{L_c}} \sum_{m_{s_0} m_{l_0}} \sum_{J_c M_c} \langle S_c M_{S_c} \tfrac{1}{2} m_{s_0} | S_0 M_{S_0} \rangle \langle L_c M_{L_c} l_0 m_{l_0} | L_0 M_{L_0} \rangle \times \langle S_c M_{S_c} L_c M_{L_c} | J_c M_c \rangle \phi(n_0 l_0 m_{s_0} m_{l_0})\, \Phi_c(L_c S_c J_c M_c) , \quad \text{(B7)}$$

where the fractional parentage coefficient $(C_{\mathrm{FP}})_{S_c L_c}^{S_0 L_0}$ takes care of the antisymmetrization. The sum over M_{S_0}, M_{L_0}, M_{S_c}, and M_{L_c} can be simplified, and (B7) becomes

$$\psi_0(L_0 S_0 J_0 M_0) = \sum_{S_c L_c} (C_{\mathrm{FP}})_{S_c L_c}^{S_0 L_0} \sum_{m_{s_0} m_{l_0}} \sum_{J_c M_c} (-)^{\omega} (\hat{J}_0 \hat{S}_0 \hat{L}_0 \hat{J}_c)^{1/2} \sum_{jm} \hat{j} \begin{pmatrix} J_0 & J_c\, j \\ M_0 & -M_c\, m \end{pmatrix} \times \begin{pmatrix} \frac{1}{2} & l_0 & j \\ m_{s_0} & m_{l_0} & m \end{pmatrix} \begin{Bmatrix} S_0 & L_0 & J_0 \\ S_c & L_c & J_c \\ \frac{1}{2} & l_0 & j \end{Bmatrix} \phi(n_0 l_0 m_{s_0} m_{l_0})\, \Phi_c(L_c S_c J_c M_c) , \quad \text{(B8)}$$

where $\omega \equiv -2S_c + \frac{1}{2} + l_0 + J_0 - 2M_0 - M_c$ and $\hat{A} \equiv 2A+1$. For the continuum wave function we introduce the partial-wave expansion:

$$\phi_{\vec{k}'}^{m_s}(\vec{r}) = (k'r)^{-1} \sum_{l'=0}^{\infty} \sum_{m'} 4\pi i^{l'} P_{l'}(k'r) \times Y_{l'm'}(\hat{r})\, Y_{l'm'}^{*}(\hat{k}')\, \chi_{1/2}^{m_s} , \quad \text{(B9)}$$

where $P_{l'}(k'r)$ is the reduced radial continuum wave function. The bound-state single-electron wave function is

$$\phi(n_0 l_0 m_{s_0} m_{l_0}) = r^{-1} P_{n_0 l_0}(r)\, Y_{l_0 m_{l_0}}(\hat{r})\, \chi_{1/2}^{m_{s_0}} , \quad \text{(B10)}$$

where $P_{n_0 l_0}(r)$ is the reduced radial bound-state wave function. The antisymmetrized final state can be written explicitly as

$$\mathcal{A}\left[\phi_{\vec{k}'}^{m_s} \Phi_c(L_c S_c J_c M_c)\right] = \frac{1}{\sqrt{N}} \left(1 - \sum_{j=2}^{N} P_{1j}\right) \times \Phi_c(L_c S_c J_c M_c;\, 234\cdots N)\, \phi_{\vec{k}'}^{m_s}(1) , \quad \text{(B11)}$$

where P_{1j} is the exchange operator for the first and jth electrons.

To evaluate the matrix element I, Eq. (B5), we shall choose $\vec{K}$ as the z axis. Then we have

$$e^{i\vec{K}\cdot\vec{r}} = (4\pi)^{1/2} \sum_{p} (2p+1)^{1/2} j_p(Kr)\, Y_{p0}(\hat{r}) . \quad \text{(B12)}$$

Thus (B5) becomes

$$I=(4\pi)^{1/2}\sum_p (2p+1)^{1/2}\langle \mathcal{A}[\phi_{\vec{k}'}^{m_s}\Phi_c(L_cS_cJ_cM_c)]$$
$$\times|j_p(Kr_1)\,Y_{p0}(\hat{r}_1)|\psi_0(L_0S_0J_0M_0)\rangle\ . \quad \text{(B13)}$$

We substitute (B11) and (B8) into (B13). In (B8), any one of N electrons can be in $\phi(n_0l_0m_{s_0}m_{l_0})$, and hence we choose the first electron. Then provided that the bound and continuum wave functions are orthogonal to each other (which is true if they are solutions in the same potential), the only contribution comes from the first term of (B11), and we have (assuming Φ_c is normalized to unity)

$$I=\left(\frac{4\pi}{N}\right)^{1/2}\sum_p (2p+1)^{1/2}\,\langle\phi_{\vec{k}'}^{m_s}(1)\,\Phi_c(L_cS_cJ_cM_c)|\,Y_{p0}(\hat{r}_1)j_p(Kr_1)|\,\psi_0(L_0S_0J_0M_0)\rangle$$
$$=\left(\frac{4\pi}{N}\right)^{1/2}(C_{\rm FP})\,{}^{S_0L_0}_{S_cL_c}(-)^{\omega}(\hat{J}_0\hat{S}_0\hat{L}_0\hat{J}_c)^{1/2}\sum_p(\hat{p})^{1/2}\sum_{m_{s_0}m_{l_0}}\sum_{jm}\hat{j}\begin{pmatrix}J_0 & J_c & j\\ M_0 & -M_c & m\end{pmatrix}$$
$$\times\begin{pmatrix}\frac{1}{2} & l_0 & j\\ m_{s_0} & m_{l_0} & m\end{pmatrix}\begin{Bmatrix}S_0 & L_0 & J_0\\ S_c & L_c & J_c\\ \frac{1}{2} & l_0 & j\end{Bmatrix}\langle\phi_{\vec{k}'}^{m_s}|\,Y_{p0}j_p(Kr)|\,\phi(n_0l_0m_{s_0}m_{l_0})\rangle\ . \quad \text{(B14)}$$

The matrix element in (B14) can be calculated using (B9) and (B10). We find

$$I=\frac{4\pi}{k'}\frac{1}{\sqrt{N}}(C_{\rm FP})\,{}^{S_0L_0}_{S_cL_c}(-)^{\omega}(\hat{J}_0\hat{S}_0\hat{L}_0\hat{J}_c)^{1/2}\sum_p\hat{p}\sum_{m_{l_0}}\sum_{jm}\hat{j}\begin{pmatrix}J_0 & J_c & j\\ M_0 & -M_c & m\end{pmatrix}\begin{pmatrix}\frac{1}{2} & l_0 & j\\ m_s & m_{l_0} & m\end{pmatrix}$$
$$\times\begin{Bmatrix}S_0 & L_0 & J_0\\ S_c & L_c & J_c\\ \frac{1}{2} & l_0 & j\end{Bmatrix}\sum_{l'=0}^{\infty}i^{l'}\,Y^*_{l'm(l_0)}(\hat{k}')\,(\hat{l}'\,\hat{l}_0)^{1/2}\begin{pmatrix}l' & p & l_0\\ 0 & 0 & 0\end{pmatrix}\begin{pmatrix}l' & p & l_0\\ -m_{l_0} & 0 & m_{l_0}\end{pmatrix}g^p_{l'l_0}(k';K)\ , \quad \text{(B15)}$$

[where $m(l_0)$ is identical to m_{l_0} and is used in subscripts for typesetting reasons] where

$$g^p_{l'l_0}(k';K)=\langle r^{-1}P_{l'}(k'r)|\,j_p(Kr)|\,r^{-1}P_{n_0l_0}(r)\rangle\ . \quad \text{(B16)}$$

Using (B15) we find

$$\sum_{M_0M_cm_s}\int d\Omega_{\vec{k}'}|I|^2=\left(\frac{4\pi}{k'}\right)^2\frac{1}{N}C^2_{\rm FP}\,\hat{J}_0\hat{S}_0\hat{L}_0\hat{J}_c\hat{l}_0\sum_{p\bar{p}}\hat{p}\hat{\bar{p}}\sum_{l'}\hat{l}'\,g^p_{l'l_0}g^{\bar{p}*}_{l'l_0}\begin{pmatrix}l' & p & l_0\\ 0 & 0 & 0\end{pmatrix}\begin{pmatrix}l' & \bar{p} & l_0\\ 0 & 0 & 0\end{pmatrix}$$
$$\times\sum_{\substack{M_0M_cm_s\\ m_{l_0}\bar{m}_{l_0}}}\begin{pmatrix}l' & p & l_0\\ -m_{l_0} & 0 & m_{l_0}\end{pmatrix}\begin{pmatrix}l' & \bar{p} & l_0\\ -\bar{m}_{l_0} & 0 & \bar{m}_{l_0}\end{pmatrix}\sum_{\substack{jm\\ \bar{j}\bar{m}}}\hat{j}\hat{\bar{j}}\begin{pmatrix}J_0 & J_c & j\\ M_0 & -M_c & m\end{pmatrix}\begin{pmatrix}J_0 & J_c & \bar{j}\\ M_0 & -M_c & \bar{m}\end{pmatrix}$$
$$\times\begin{pmatrix}\frac{1}{2} & l_0 & j\\ m_s & m_{l_0} & m\end{pmatrix}\begin{pmatrix}\frac{1}{2} & l_0 & \bar{j}\\ m_s & \bar{m}_{l_0} & \bar{m}\end{pmatrix}\begin{Bmatrix}S_0 & L_0 & J_0\\ S_c & L_c & J_c\\ \frac{1}{2} & l_0 & j\end{Bmatrix}\begin{Bmatrix}S_0 & L_0 & J_0\\ S_c & L_c & J_c\\ \frac{1}{2} & l_0 & \bar{j}\end{Bmatrix}\ . \quad \text{(B17)}$$

The sums over the magnetic quantum numbers can be done explicitly; then (B17) reduces to

$$\sum_{M_0M_cm_s}\int d\Omega_{\vec{k}'}|I|^2=\left(\frac{4\pi}{k'}\right)^2\frac{1}{N}C^2_{\rm FP}\,\hat{J}_0\hat{S}_0\hat{L}_0\hat{J}_c\sum_p\hat{p}\sum_{l'}\hat{l}'\,|g^p_{l'l_0}|^2\begin{pmatrix}l' & p & l_0\\ 0 & 0 & 0\end{pmatrix}^2\sum_j\hat{j}\begin{Bmatrix}S_0 & L_0 & J_0\\ S_c & L_c & J_c\\ \frac{1}{2} & l_0 & j\end{Bmatrix}^2\ . \quad \text{(B18)}$$

Substituting (B18) into (B6) we obtain Eq. (16) of the text.

*Work supported by the National Science Foundation.

†On leave from the California State University, Los Angeles, Calif. 90032.

[1]A. E. S. Green, D. L. Sellin, and A. S. Zachor, Phys. Rev. 184, 1 (1969).

[2]J. E. Purcell, R. A. Berg, and A. E. S. Green,

Phys. Rev. A 2, 107 (1970); 3, 509 (1971).
[3]P. S. Ganas and A. E. S. Green, Phys. Rev. A 4, 182 (1971).
[4]T. Sawada, J. E. Purcell, and A. E. S. Green, Phys. Rev. A 4, 193 (1971).
[5]R. A. Berg and A. E. S. Green, Advan. Quantum Chem. (to be published).
[6]C. E. Moore, *Atomic Energy Levels*, Natl. Bur. Std. (U.S.) Circ. No. 467 (U. S. GPO, Washington, D.C., 1958), Vol. I.
[7]A. Messiah, *Quantum Mechanics*, Vol. II (North-Holland, Amsterdam, 1958), Appendix C.
[8]A. R. Edmonds, *Angular Momentum in Quantum Mechanics* (Princeton U. P., Princeton, N. J., 1957).
[9]B. W. Shore and D. H. Menzel, *Principles of Atomic Spectra* (Wiley, New York, 1968).
[10]Y. K. Kim, M. Inokuti, G. E. Chamberlain, and S. R. Mielczarek, Phys. Rev. Letters 21, 1146 (1968).
[11]E. J. McGuire, Sandia Labs. Res. Rept. No. SC-RR-70-406, 1971 (unpublished).
[12]A. E. S. Green and S. K. Dutta, J. Geophys. Res. 72, 3933 (1967).
[13]E. J. Stone and E. C. Zipf, Phys. Rev. A 4, 610 (1971).
[14]U. Fano and J. W. Cooper, Phys. Rev. 137, A1364 (1965).
[15]P. S. Kelly, J. Quant. Spectry. Radiative Transfer 4, 117 (1964).
[16]A. B. Prag, C. E. Fairchild, and L. C. Clarn, Phys. Rev. 137, A1358 (1965).
[17]F. A. Morse and F. Kaufman, J. Chem. Phys. 42, 1785 (1965).
[18]D. A. Parkes, L. F. Keyser, and F. Kaufman, Astrophys. J. 149, 217 (1967).
[19]G. Boldt and F. Labuhn, Z. Naturforsch. A22, 1613 (1967).
[20]C. Lin, D. A. Parkes, and F. Kaufman, J. Chem. Phys. 53, 3896 (1970).
[21]B. D. Savage and G. M. Lawrence, Astrophys. J. 146, 940 (1966).
[22]J. E. Hesser, J. Chem. Phys. 48, 2518 (1968).
[23]G. M. Lawrence and M. George, Phys. Rev. 175, 40 (1968).
[24]W. L. Fite and R. T. Brackmann, Phys. Rev. 113, 815 (1959).
[25]A. Boksenberg, thesis (University of London, 1961) (unpublished).
[26]M. J. Seaton, Phys. Rev. 113, 814 (1959).
[27]L. J. Kieffer, Compilation of Low Energy Electron Collision Cross Section Data, Part I, JILA Information Center Rept. No. 6, University of Colorado, 1969 (unpublished).

PHYSICAL REVIEW A VOLUME 6, NUMBER 6 DECEMBER 1972

Dissociative Excitation of Molecular Hydrogen by Electron Impact*

Martin Misakian† and Jens C. Zorn
Randall Laboratory of Physics, The University of Michigan, Ann Arbor, Michigan 48104
(Received 23 August 1971; revised manuscript received 26 June 1972)

Dissociative excitation of molecular hydrogen can proceed via the process $H_2+e\rightarrow H(2s)+H+e$ and yield metastable H(2s) atoms that have kinetic energies near 0.3 eV ("slow") or near 4 eV ("fast"). The dissociation process has been studied using a pulsed electron gun with an energy resolution of ± 0.3 eV and using a metastable atom detector capable of viewing H(2s) atoms with an angular resolution of 1° over a range 60°–120° with respect to the electron-beam direction. The measurement of the angular intensity distribution gives information about the final states that are involved in the dissociation process. (i) For slow H(2s) atoms, the electron energy threshold for production of the least energetic of the slow metastable atoms is 14.6 ± 0.3 eV. The excitation function and the angular distribution of the slow H(2s) atoms suggest that the $B'\,^1\Sigma_u^+$, $e\,^3\Sigma_u^+$, $D\,^1\Pi_u^+$, and $d\,^3\Pi_u^+$ excited states are involved in the formation of these metastable fragments. (ii) For fast H(2s) atoms, the electron energy threshold for production of the least energetic of the fast H(2s) atoms is near 29 eV. The angular distribution data would indicate that these atoms arise from a Π_u state; the form of the excitation function indicates that the parent state has a multiplicity of 1. The change in energy distribution of the fast H(2s) atoms, measured as a function of electron-gun voltage, supports the view that the $^1\Pi_u$ state is a previously unreported doubly excited state that has an asymptotic energy of 24.9 eV.

I. INTRODUCTION

Recently Leventhal, Robiscoe, and Lea[1] employed a time-of-flight (TOF) technique to measure the energy distributions of metastable H(2s) atom fragments that were produced via the process

$$H_2+e\rightarrow H(2s)+H+e\ .$$

H(2s) atoms were produced by pulsing a simple triode electron gun in an H_2 atmosphere. The metastable atoms moved translationally with kinetic energy released during the dissociation process and after some collimation entered a "quench" region 10 cm away. A strong electric field was applied in this region which mixed the $2S_{1/2}$ and $2P_{1/2}$ states causing a decay to the ground state.